Combustion and Flame 162 (2015) 41–49

Contents lists available at ScienceDirect

Combustion and Flame

journal homepage: www.elsevier.com/locate/combustflame

Combustion inhibition and enhancement of premixed methane–air flames by halon replacements ☆

John L. Pagliaro [a], Gregory T. Linteris [b,*], Peter B. Sunderland [a], Patrick T. Baker [c]

[a] Dept. of Fire Protection Engineering, University of Maryland, College Park, MD 20742, USA
[b] Fire Research Division, National Institute of Standards and Technology, Gaithersburg, MD 20899, USA
[c] The Boeing Company, Seattle, WA 98124, USA

ARTICLE INFO

Article history:
Received 28 April 2014
Received in revised form 30 June 2014
Accepted 7 July 2014
Available online 22 August 2014

Keywords:
Fire suppression
Halon 1301
Aircraft cargo bay fire protection
Halon replacement
Refrigerant flammability
Explosion suppression

ABSTRACT

Apparent combustion enhancement by some halon replacement fire suppressants (proposed for use in aircraft cargo bays) has been observed in full-scale, constant-volume tests at the FAA. In order to explore the phenomena, laboratory-scale constant-volume combustion experiments were performed. The maximum explosion pressure and burning velocity were measured for methane–air flames with added CF_3Br (Halon 1301), $C_6F_{12}O$ (Novec 1230), $C_3H_2F_3Br$ (2-BTP), and C_2HF_5 (HFC-125). The explosion pressure, for initially stoichiometric flames, was increased mildly (up to 11% and 6%) with $C_6F_{12}O$ and C_2HF_5 added at low concentrations, while at lean conditions ($\Phi = 0.6$), it was increased about 50% for added $C_6F_{12}O$, $C_3H_2F_3Br$, or C_2HF_5, at agent volume fractions $X_a = 0.02$, 0.03, and 0.06. The burning velocity for initially stoichiometric flames was always decreased with addition of any of the agents, whereas, for the lean conditions, it increased with added $C_6F_{12}O$ or C_2HF_5 (32% and 14%, at $X_a = 0.01$ and 0.03). Burning velocities at higher initial pressure (3 bar) and temperature (400 K) showed lower inhibition effectiveness (than at ambient conditions) for the stoichiometric flames, and larger enhancement for the lean flames (and the effect was due primarily to the temperature increase). CF_3Br did not increase the explosion pressure or burning velocity for any of the tested conditions. Equilibrium calculations were used to interpret the experiments. The present work is consistent with the FAA results and previous analysis of the full-scale tests.

Published by Elsevier Inc. on behalf of The Combustion Institute.

1. Introduction

Halon 1301 (CF_3Br) is a very effective fire suppressant, but has been banned by the Montreal Protocol [1] because of its high ozone depletion potential (ODP). A critical-use exemption of recycled CF_3Br has been granted for aircraft crew compartments, engine nacelles, cargo bays, dry bays, and fuel tanks [2]. Nonetheless, the European Union is requiring replacement of CF_3Br in newly constructed aircraft by 2018 and in existing aircraft by 2040.

Three potential drop-in halon replacements were tested by the Federal Aviation Administration (FAA) for use in cargo bays, and all failed the FAA Aerosol Can Test (FAA-ACT) [3], which is one component of the minimum performance standard for halon replacements [4]. The aerosol can test simulates the explosion of an aerosol can caused by a fire in the cargo bay. In the FAA-ACT, air and suppressant are premixed in a simulated cargo bay compartment (a pressure vessel, 11.4 m^3 in volume), in which a fast-acting valve releases the simulated can contents (a two-phase spray of alcohol, propane, and water) past a continuous high-voltage DC arc. In the absence of suppressant, the pressure rise in the chamber is about 2 bar. Through repeated tests at different agent volume fractions X_a, the inerting concentration of an agent is determined as the value of X_a required to prevent significant pressure rise. The standard also requires that an agent, when added at sub-inerting concentrations, cannot produce a higher pressure rise than the uninhibited case. Unfortunately, all of the agents tested ($C_6F_{12}O$, Novec 1230, FK-5-1-12, $CF_3CF_2C(=O)CF(CF_3)_2$; $C_3H_2F_3Br$, 2-BTP, CH_2CBrCF_3; and C_2HF_5, CHF_2CF_3, HFC-125), failed this element of the test, whereas Halon 1301 (CF_3Br) did not [3,5].

Experimental and numerical investigations of laboratory flames have described enhanced combustion with addition of halogenated suppressants, as outlined in Ref. [6]. The phenomena include

☆ Official contribution of NIST, not subject to copyright in the United States. Certain commercial equipment, instruments, and materials are identified in this paper to adequately specify procedure. Such identification does not imply recommendation or endorsement by the National Institute of Standards and Technology.

* Corresponding author. Address: National Institute of Standards and Technology, Engineering Laboratory, Gaithersburg, MD 20899, USA. Fax: +1 301 975 4052.
E-mail address: linteris@nist.gov (G.T. Linteris).

http://dx.doi.org/10.1016/j.combustflame.2014.07.006
0010-2180/Published by Elsevier Inc. on behalf of The Combustion Institute.

increased total heat release, widened lean flammability limits, decreased ignition delay, and increased pressure rise. Most of the early work documented the effects, but did not analyze the causes. In more recent work [6–12], numerical combustion simulations have been applied to gain insight using recently developed (or updated) kinetic mechanisms [10,13–18]. The studies have concluded that exothermic reaction of the fire suppressants adds energy to the constant volume system, increasing the overpressure. To obtain the observed pressure rise in the FAA-ACT, agent reaction is shown to occur under very fuel-lean equivalence ratios (Φ, based on the aerosol can fuel only), nearly corresponding to pure agent and air. Kinetic calculations have indicated that addition of the agent to fuel-lean flames can increase not only the energy release, but the rate of reaction as well. Nonetheless, no laboratory-scale experiments have been conducted to validate the explanations or to explore the combustion enhancement observed in the FAA tests for the new agents $C_6F_{12}O$ and $C_3H_2F_3Br$ (and experiments for C_2HF_5 are limited [19,20]). Experimental studies of the influence of halogenated suppressants on laminar burning velocity exist [21–27], but very little data are available for agent addition to very lean hydrocarbon–air mixtures (which are of most interest with regard to the FAA tests). Previous work has shown the effectiveness of the agents $C_6F_{12}O$ and $C_3H_2F_3Br$ in standard tests for fire suppressant efficacy [28–31], but there are no data for their effect on burning velocity (a traditional method of quantifying flame inhibition effectiveness [32]).

In the present work, the agents used in the FAA-ACT (CF_3Br, $C_6F_{12}O$, $C_3H_2F_3Br$, and C_2HF_5) are added at various sub-inerting concentrations to stoichiometric and lean methane–air flames in a laboratory-scale constant volume combustion chamber to determine their influence on the maximum pressure rise and burning velocity. The effects of compressive heating on the burning velocity are also determined. The goals of the present work are to test the concepts developed via numerical simulations and analysis of the FAA tests [6,7,10], reproduce the phenomena observed in the complex full-scale FAA experiments, and explore if the laboratory-scale experiment can be used as a screening tool for cargo bay halon replacements. Although the FAA-ACT fuel is composed of propane, ethanol, and water, methane was used to simplify the experimental procedure, and to reduce the potential influence of flame stretch and radiative heat loss from soot formation. Additionally, since the experimental data are among the first to examine the effect of added $C_6F_{12}O$ and $C_3H_2F_3Br$ on premixed flames, performing experiments with a simple hydrocarbon seems appropriate (previous work showed the inhibition effectiveness of halogenated suppressants to be relatively insensitive to the hydrocarbon fuel type [33]).

2. Experimental

2.1. Apparatus and procedure

A schematic diagram of the constant volume apparatus is shown in Fig. 1. The stainless steel (316) spherical vessel is similar to previous designs [34–37], with an inner diameter of 15.24 cm, volume of 1.85 L, wall thickness of 2.54 cm, and is equipped with electrodes, an absolute pressure gage, a dynamic pressure sensor, and a thermocouple. The experiment can provide the flammability limits, explosion pressure (constant-volume), and rate of pressure rise; further processing of the latter can be used to obtain the laminar burning velocity (1-D spherical) as a function of initial pressure and temperature (which increase as the unburned gases are compressed).

A vacuum pump reduces chamber pressure below 0.1 Torr prior to reactant addition. Test mixtures are prepared in the chamber using the partial pressure method, following injection of first liquid then gaseous reactants. Component partial pressures are determined with an absolute pressure transducer (Omega, PX811; claimed accuracy of 0.1% of reading) that is periodically calibrated against a Baratron 627D (claimed accuracy of 0.12%) and a Wallace & Tiernan 1500 pressure gage (claimed accuracy of 0.066%). Liquid suppressants ($C_6F_{12}O$ and $C_3H_2F_3Br$) are injected using a syringe and a gas-tight septum separated from the chamber by a ball valve (to ensure leak-free operation during the experiment).

The ignition system initiates reaction either via an electrical spark, or hot-wire heating. The present work uses only the former (a capacitive discharge ignition system, based on the work of Shepherd et al. [38]). A 1–15 kV power supply (Acopian) and custom-made capacitor banks (1–50 nF) provide variable ignition energies, with an estimated operating range of 0.05–500 mJ. Two tungsten electrodes form a gap in the center of the chamber. Thin electrodes (0.4 mm diameter) minimize heat loss from the flame, and the spark gap is adjustable (2 mm, typical).

The sample gases are CH_4 (Matheson Tri-Gas, 99.97% purity), CF_3Br (Great Lakes Chemical Corp., 99.6% purity), $C_6F_{12}O$ (3M, >99% purity), $C_3H_2F_3Br$ (American Pacific Corp., >99% purity), and C_2HF_5 (Allied Signal Chemicals, 99.5% purity). The air is house compressed air (filtered and dried) that is additionally conditioned with a 0.01 μm filter, carbon filter, and a desiccant bed to remove small aerosols, organic vapors, and water vapor before use. The relative humidity of the air, measured with a humidity gage (TSI VELOCICALC, 8386), is less than 2% for all tests.

For a test, the reactants are added, followed by a 5 min mixing and settling time [34]. Ignition is attempted several times, while gradually increasing the capacitor charging voltage, until ignition occurs. This ensures the ignition energy is within an order of magnitude of the minimum value. (Note that for stoichiometric iso-octane–air mixtures, Marshall et al. [39] found that the burning velocity was insensitive to the ignition energy for values up to 1000 times the minimum ignition energy.) The explosion pressure is recorded at 4000 Hz. with a dynamic pressure sensor (PCB Piezotronics, 101A06; claimed accuracy of 0.1% of reading). The product gases are immediately purged to vacuum via a large flow of N_2 (to minimize acid gas exposure to, and heating of, the experiment), and the chamber is allowed to cool for 20 min before the next experiment. Laminar burning velocity is determined from the pressure trace using a thermodynamic model, developed by Metghalchi and Keck [34,40] and further refined by others [35,41]. A brief overview of the method follows.

2.2. Burning velocity from the pressure trace

The contents of the chamber are divided into burned and unburned zones separated by a reaction sheet, assumed to be of zero thickness, spherical, and smooth (no instabilities). Initially, the unburned gas is considered mixed and at rest. As the unburned gases react, a spatially uniform increase in pressure occurs. The burned gas is in chemical equilibrium and both the burned and unburned gases are considered as ideal, semi-perfect gases. Both zones are adiabatic, and the unburned gas is isentropically compressed as the mixture reacts in the flame sheet.

With these assumptions, the instantaneous flame radius and burning velocity can be expressed in terms of the chamber pressure by applying conservation of mass. The results are given in Eqs. (1) and (2) (detailed formulation of the equations can be found in Refs. [34,41]),

$$r_f = R[1 - (1 - x_b)(P_0/P)^{1/\gamma_u}]^{1/3} \quad (1)$$

$$S_L = R/3(R/r_f)^2(P_0/P)^{1/\gamma_u}(dx_b/dt) \quad (2)$$

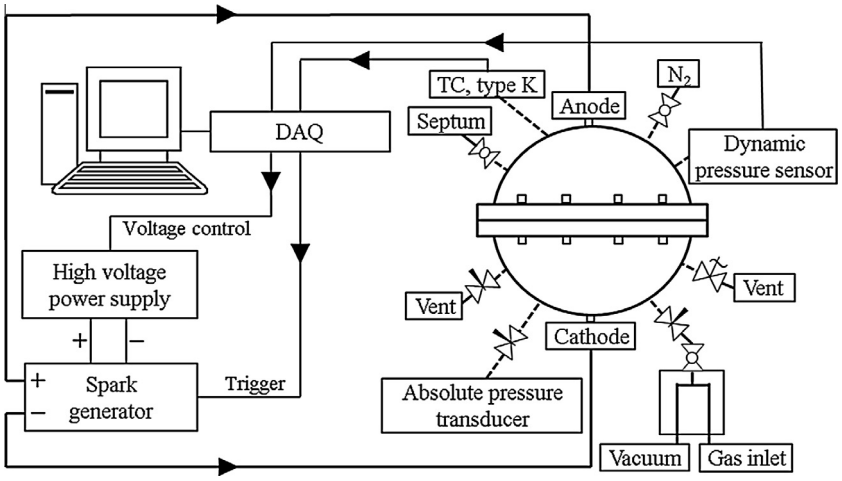

Fig. 1. Schematic diagram of the experimental apparatus.

in which r_f is the flame radius, S_u is the laminar burning velocity, R is the chamber radius, x_b is the mass fraction of burned gas, P is the instantaneous pressure, P_0 is the initial pressure, and γ_u is the unburned gas specific heat ratio. To determine burning velocity, the mass fraction of burned gas x_b must be related to the chamber pressure (for simplification, early studies applied a linear relationship [42]). Alternatively, a thermodynamic closed system analysis on the contents within the chamber can be performed. A two-zone approach is used in the present work. The burned gas zone also can be modeled using incremental shell volumes [43,44], allowing burned gas density and temperature gradients; nonetheless, since previous studies have shown that inclusion of the gradients has negligible effect on the burning velocity [40,41], we retain the two-zone model. The fraction of mass burned x_b is found from simultaneous solution of the conservation of mass and energy equations given in Eqs. (3) and (4), applied for the two zones,

$$\frac{V}{M} = \int_0^{x_b} v_b dx + \int_{x_b}^{1} v_u dx \tag{3}$$

$$\frac{E}{M} = \int_0^{x_b} e_b dx + \int_{x_b}^{1} e_u dx \tag{4}$$

where V is the volume of the chamber, E is the total internal energy of the gases in the chamber, M is the mass of the initial gas in the chamber, e and v are the internal energy and specific volume of the gas, and the subscripts b and u refer to the burned and unburned gas.

Thermodynamic data for the unburned and burned gases are required for model implementation. Data for hydrocarbon–air species (CH_4, O_2, N_2, CO_2, H_2O, CO, NO, OH, H_2, and O) are taken from GRI-mech 3.0 [45], fluorinated species ($C_6F_{12}O$, C_2HF_5, F, HF, CF_4, and CF_2O) from the NIST HFC mechanism [13,17], and brominated species (CF_3Br, $C_3H_2F_3Br$, Br, HBr, and Br_2) from Babushok et al. [14,46]. Hydrocarbon–air product species are included for all mixtures, along with fluorinated products for test containing $C_6F_{12}O$ or C_2HF_5. Additional brominated products are included for tests with CF_3Br or $C_3H_2F_3Br$.

The unburned gas properties are related to the chamber pressure through isentropic compression:

$$T_u = T_{u0}\left(\frac{P}{P_0}\right)^{(\gamma_u - 1)/\gamma_u} \tag{5}$$

in which T_{u0} is the initial unburned temperature. Since γ_u is a function of the unburned gas temperature T_u and the initial mixture composition, T_u and γ_u are solved iteratively at each pressure increment. The properties of the unburned gas mixture, v_u and e_u, are determined from the mixture composition and temperature.The remaining unknowns in the conservation equations (v_b, e_b, and x_b) are found through iteration of T_b (v_b and e_b are functions of temperature) and x_b at each pressure increment, until the proper values of T_b and x_b are obtained. Burned gas species concentrations, required for the determination of v_b and e_b, are estimated using a constant volume equilibrium calculation performed via the CEA2 routine of Gordon and McBride [47], with T_{u0} and P_0 as initial conditions. The enthalpies of formation of $C_6F_{12}O$, C_2HF_5, and $C_3H_2F_3Br$ (required for CEA2 calculation) are from Refs. [6,10,13]. Once $x_b(P)$ is known, the burning velocity $S_u(P, T_u)$ is calculated over the experimental range of pressure and temperature using Eq. (2).

2.3. Data reduction

Figure 2 shows a typical pressure trace (solid line) from an experiment (CH_4–air, $\Phi = 1.0$), along with T_b, T_u, and r_f, which are outputs of the two-zone model calculation. Only a portion of the pressure data is used for obtaining burning velocity, as denoted by the thick line on the pressure trace. For small r_f, the flame behavior is affected by flame stretch and the ignition process, and for large r_f, by heat losses to the walls and cellular instabilities;

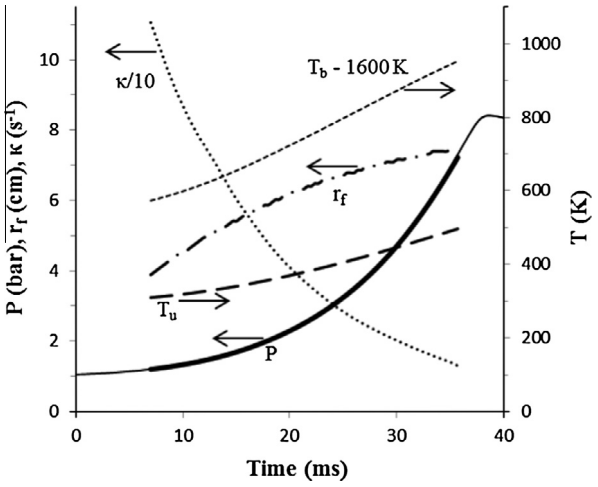

Fig. 2. Experimental pressure trace P, flame radius r_f, flame stretch rate κ, and gas temperature (unburned T_u and burned T_b) as a function of time.

hence, typically only the central 75% of the pressure data are used. Spherically propagating flames are subject to stretch rates inversely proportional to the flame radius [48],

$$\kappa = \frac{2}{r_f}\frac{dr_f}{dt} \tag{6}$$

where κ is the stretch rate and dr_f/dt is the flame front velocity. Figure 2 also shows the stretch rate for this experiment. To reduce stretch effects (as well as the transient caused by the ignition), data are neglected for small flame radii, $r_f < 3.8$ cm (i.e., $r_f < R/2$, as proposed by Elia et al. [49], and adopted by others [39,43,50]). For $r_f/R = 0.5$, peak stretch rates range between 110 s^{-1} for uninhibited stoichiometric methane–air and 20 s^{-1} for inhibited cases with burning velocities near 6 cm/s. To avoid the effects of heat losses to the walls, only data up to dP/dt_{max} (i.e., the inflection point in the $P(t)$ curve in Fig. 2) are used, following the recommendations in Refs. [51,52].

A single experiment provides burning velocity data for a range of pressure and temperature of the unburned gas, and these data are fit to the equation [33]:

$$S_L = S_{L,0}\left(\frac{T}{T_0}\right)^{\alpha}\left(\frac{P}{P_0}\right)^{\beta} \tag{7}$$

in which S_L is the laminar burning velocity, P_0 is the initial pressure, T_0 is the initial temperature, $S_{L,0}$ is the laminar burning velocity at the initial conditions; α, β, and $S_{L,0}$ are the fitting parameters. In the experiments performed, T_0 is 296 ± 2 K, and P_0 is 0.868 bar, 1 bar, and 1.13 bar, (to provide more data for the curve fit). Individual tests were repeated twice for each initial pressure and the raw data from each test was included in the fitting to Eq. (7).

Figure 3 shows the burning velocity of stoichiometric methane–air as a function of unburned gas temperature and chamber pressure. The light grey surface is the fit following Eq. (7), and the darker grey data points (and lines through them) are the S_L values at each combination of unburned gas pressure and temperature for a specific run, to which Eq. (7) is fit. In discussions following, S_L is presented at ambient conditions and under compressive heating, as obtained from Eq. (7) (and shown as black dots in Fig. 3). Note that the presented results are interpolations, or small extrapolations, from the experimental data, as illustrated in Fig. 3.

In the present method, spherical flame propagation is a critical condition for accurate determination of S_L from the pressure trace. Buoyancy can distort the shape of the flame, especially for slow burning mixtures (which are of particular interest in the present work). Takizawa et al. [35] estimated the minimum burning velocity measurable without error associated with buoyancy. They performed experiments in a spherical chamber, using the pressure rise to determine burning velocity. Separate experiments were performed in a cylindrical chamber with visual access to provide comparison. The shape of the flame front was recorded with high speed video and the burning velocity was calculated using the constant-pressure method [53,54]. To minimize the effects of buoyancy, as recommended by Pfahl et al. [55], the rate of change of the flame radius with respect to time was traced in the two horizontal directions. Results [35] showed that burning velocities as low as 6 cm/s could be measured with the constant-volume method. In the present work, cellular instabilities, which also invalidate the spherical flame assumption, are monitored through inspection of the S_L data of individual test runs. The onset of cellular instabilities is typically detected via a distinct increase in S_L [39,43], and these data (if occurring) are omitted during the experimental data fitting.

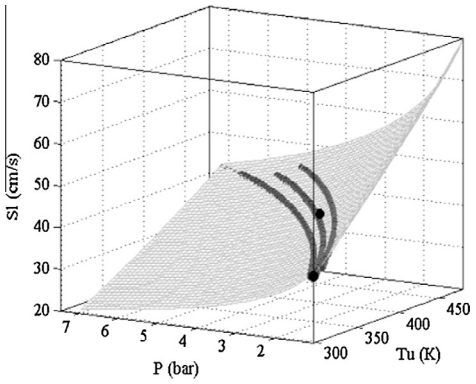

Fig. 3. Three dimensional plot of burning velocity as a function of pressure P and unburned gas temperature T_u. The dark grey dots represent the data from six experiments, two of which are performed at each initial pressure. The light grey surface represents the fitted results using Eq. (7) and the black dots are the reported S_L at ambient ($T_0 = 298$ K, $P_0 = 1$ bar) and compressed ($T_0 = 400$ K, $P_0 = 3$ bar) conditions.

2.4. Uncertainties

The uncertainty analysis consists of individual uncertainty components and root-sum-of-squares (RSS) components [56]. Uncertainties in the measured parameters are reported as *expanded uncertainties*: ku_c, from a combined standard uncertainty (estimated standard deviation) u_c, and a coverage factor $k = 2$ (level of confidence approximately 95%). Likewise, when reported, the relative uncertainty is ku_c/X. Uncertainties in initial temperature and pressure, dynamic and peak pressure rise, agent volume fraction, equivalence ratio, and the burning velocity calculation and fitting to Eq. (7) are considered. The expanded relative uncertainties related to mixture composition are as follows: 0.5% for equivalence ratio; and 0.4%, 0.8%, and 4% for the reactant mole fractions of air, CH_4, and agent. Relative uncertainties of the dynamic and peak pressure rise, initial pressure, and initial temperature are 1.3%, 0.5%, and 1%. The expanded relative uncertainty for experimentally determined burning velocities is 6%.

3. Results

3.1. Experimental validation

To validate the accuracy of the experimental facility and the post-processing procedure, the burning velocity of methane–air flames was determined over a range of equivalence ratios (0.6–1.3). Figure 4 compares the present results to published data at standard (298 K, 1 bar; lower curve) and compressed (400 K, 3 bar; upper curve) conditions. The solid black squares show the present data, other black symbols show data collected using the same experimental technique [35,36], blue symbols show stretch-corrected data from spherical flames [26,57,58], and red symbols show stretch-corrected data from counter-flow flames [59,60].

For the initially ambient mixtures, the burning velocities are in excellent agreement with previous results using the constant-volume method with a similarly sized chamber and a two-zone model [35]. Values are within 1% at all equivalence ratios except for $\Phi = 0.7$ and $\Phi = 1.2$ where S_L is 5% higher and 3% lower (the symbols in Fig. 4 representing the data of Ref. [35] are not visible because they are so closely aligned with the larger square symbols showing the present data). Results are within 5% of Ref. [36], except at $\Phi = 1.2$ where S_L is 8.5% lower. Burning velocities are also in satisfactory agreement with stretched-corrected spherically propagating [26,57,58] and counterflow [59,60] flame data, within the scatter of reported values for the entire range of Φ. (For comparison, the same experimental P vs. t data were post-processed

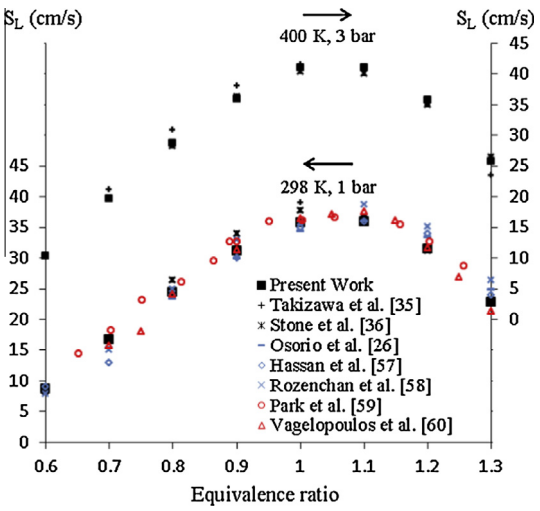

Fig. 4. Burning velocity of premixed methane–air flames at 298 K and 1 bar (lower) and 400 K and 3 bar (upper) as a function of equivalence ratio, together with previously published results.

using the linear relationship between P and x_b [42]. This technique yielded burning velocities that were roughly 8% higher than the two-zone model approach, with S_L = 38.9 cm/s at Φ = 1.0. Similar findings were reported by Refs. [52,61]; thus, the two-zone model approach was selected for post-processing the inhibited flame data.)

The upper set of symbols in Fig. 4 compares burning velocities at the compressed conditions with previous results using the same constant-volume method. The present burning velocities are in excellent agreement with the results of Stone et al. [36] and in satisfactory (±9%) agreement with Takizawa et al. [35]. Overall, the methane validation results show that the present experimental approach provides burning velocities in agreement with those of other investigations at standard and compressed (400 K, 3 bar) conditions.

3.2. Peak pressure rise

The maximum pressure rise of methane–air explosions in a closed vessel was determined with addition of CF_3Br, $C_6F_{12}O$, $C_3H_2F_3Br$, and C_2HF_5 (T_0 = 298 K, P_0 = 1 bar). Agents were added to stoichiometric flames and lean flames with a fuel–air equivalence ratio Φ of 0.6 (Φ based on uninhibited mixtures, i.e., when an agent is added, proportional quantities of methane and air are displaced). Figure 5 shows the results for the stoichiometric and lean systems. The peak pressure rise ΔP_{max} from experiments is shown, along with the calculated equilibrium ΔP_{max} and adiabatic temperature T_{ad} (calculated using CEA2, for a constant internal energy, constant volume system). The line styles denoting the results for each agent are defined via the experimental curves, and the assignment is preserved for the two sets of equilibrium curves. For reference, the uninhibited system has T_{ad} = 2599 K and ΔP_{max} = 7.94 bar at equilibrium.

For the stoichiometric system, adding CF_3Br decreases T_{ad}, whereas adding any of the other agents slightly increases T_{ad} (≈2612 K) at low X_a, and then decreases it as X_a increases, with the larger inhibitor molecules decreasing T_{ad} more. The observed increases in T_{ad} are comparable to the increase that occurs from stoichiometric to slightly rich conditions in methane–air systems (peak T_{ad} = 2615 K at Φ = 1.07).

For the stoichiometric case (left frame in Fig. 5), the equilibrium pressure (lines with no symbols) increases with addition of each agent, including CF_3Br, up to a certain value of X_a, then drops for higher X_a. The value of X_a controlling this behavior is related to the halogen X to hydrogen H ratio [X]/[H] in the premixed gases, which is equal to unity for CF_3Br, $C_6F_{12}O$, $C_3H_2F_3Br$, and C_2HF_5 at X_a = 0.09, 0.03, 0.16, and 0.09 (as indicted by the vertical lines at the top of the figure). Since X_a for [X]/[H] = 1 is off the figure when adding CF_3Br, $C_3H_2F_3Br$, and C_2HF_5 to the stoichiometric case, the equilibrium ΔP_{max} increases continuously on the figure. The increase in ΔP_{max} is caused by the increase in the number of moles of products, which overrides the lower values of T_{ad} with agent addition. For X_a above [X]/[H] = 1, the equilibrium products change (formation of COF_2 rather than HF, as a fate for F), so the number of moles of product decreases, reducing ΔP_{max}. With agent added to these stoichiometric flames, $C_6F_{12}O$, $C_3H_2F_3Br$, and C_2HF_5, have a maximum equilibrium pressures rise 2 bar, 1.5 bar, and 0.6 bar higher than with no agent, occurring at X_a = 0.03, 0.07, and 0.04. Note that the equilibrium ΔP_{max} is relatively insensitive to X_a for $C_3H_2F_3Br$, and that calculations show an increase in ΔP_{max} even for addition of CF_3Br. Moreover, the equilibrium results for inhibited methane-fueled flames are qualitatively consistent with results for inhibited propane- or aerosol can content-fueled [3] flames.

As shown in Fig. 5 (again for Φ = 1), the experimentally determined ΔP_{max} of all agents is less than the equilibrium value. For example, the uninhibited stoichiometric methane–air system has an experimental ΔP_{max} = 7.2 bar, which is close to ΔP_{max} = 7.3 bar measured by Ref. [62] and about 9% lower than the equilibrium value. To some extent, the experimental values of ΔP_{max} with added agent follow the trends in the equilibrium values, although the experimental ΔP_{max} rises more slowly than the equilibrium value, before eventually dropping rapidly. This can be caused by flame quenching (from heat losses at the wall [63] or from buoyancy [64]), by radiative heat loss, and (for these initially stoichiometric flames) by kinetic quenching of the flame reactions. While it is possible to define an extent of reaction λ based on the ratio of measured to equilibrium ΔP_{max} [63], this is of limited value in the present work since the effects interact: slower burning velocities (with inhibitor) allow more time for buoyancy to act, and buoyancy-induced quenching lowers the temperature (and hence the overall reaction rate), which can also affect the kinetic inhibition. Also, the effects are likely to depend upon the size of the sphere and degree of turbulence [65] (which are different in the FAA-ACT test). Note that while equilibrium calculations predict enhanced pressure rise with CF_3Br and $C_3H_2F_3Br$, both have none, and have much reduced pressure rise as X_a increases (likely due to kinetic inhibition by the bromine [16]). For addition to *stoichiometric flames*, $C_6F_{12}O$ and C_2HF_5 increase the experimental ΔP_{max} by 11% and 6%, at X_a = 0.02 and X_a = 0.03.

The influence of radiative heat losses in reducing the pressure rise was estimated via a calculation similar to that in Ref. [41]. In the calculation, CO_2, H_2O, and HF were considered as radiating products, and the radiative heat loss of the expanding burned gas zone was estimated. Species volume fractions and burned gas temperatures were taken from equilibrium calculations using CEA2 [47]. The emissivity of CO_2 and H_2O [66] and HF [67] were estimated based on the burned gas temperature, partial pressures, mean equivalent beam length, and chamber pressure. The thermodynamic model (developed to calculate burning velocity) was used to estimate the flame radius r_f with respect to time to provide the mean equivalent beam length (4/3 * r_f for a spherical volume). The radiative heat loss rate ($\dot{Q}_{rad} = \sigma \varepsilon A T_b^4$) was determined from the burned gas emissivity ε, burned gas temperature T_b, and flame area A. The rate was then integrated over the flame propagation time to yield the total radiative heat transfer. A chamber reflectivity of 0.25 was assumed for the stainless steel walls to account for residual buildup between cleaning. These estimates indicate that radiation

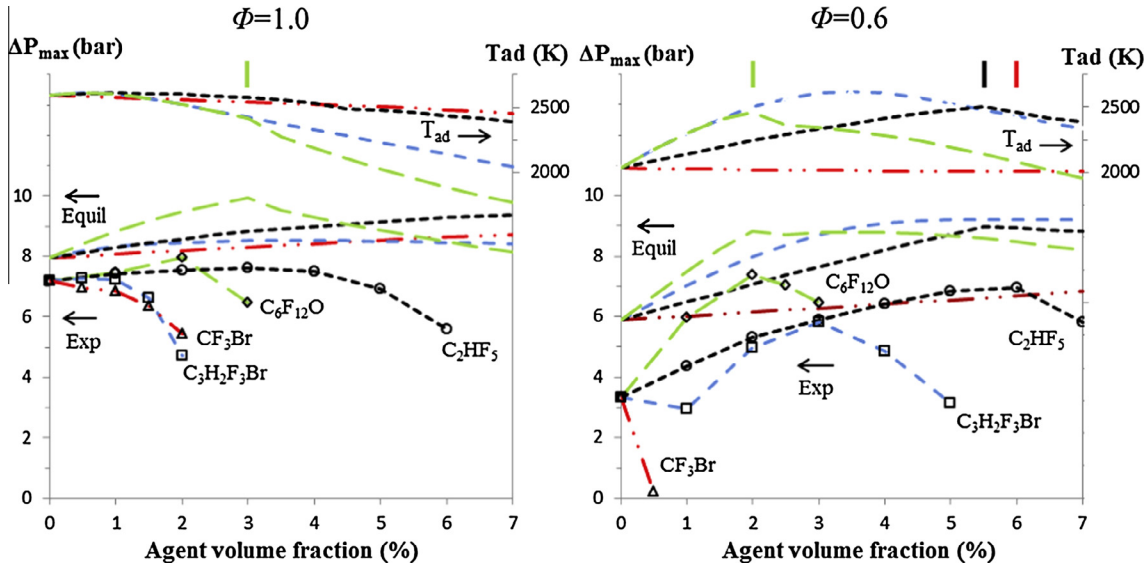

Fig. 5. Pressure rise (left scale) and adiabatic temperature (right scale) in constant-volume combustion sphere with agents added to methane–air flames (Φ = 1.0, left frame, Φ = 0.6, right frame). Lines: equilibrium calculations; lines with symbols: experiments.

ranges from 2–12% of the total heat release (highest for strongly inhibited lean mixtures), which is significantly higher than the 1% reported in Ref. [41]. The larger values are primarily due to the lower heat release rates of the slower burning flames. Accordingly, since the experimental ΔP_{max} (i.e., heat release) is typically 30–60% lower than the equilibrium values (at the highest level of agent addition), as compared to the radiant losses of up to 12%, wall quenching (enhanced by buoyant flow) seems to be the primary cause for the lower experimental ΔP_{max}.

Results for lean methane–air mixtures (Φ = 0.6) are shown in the right frame of Fig. 5. For reference, the equilibrium adiabatic temperature and pressure rise for an uninhibited methane–air mixture at Φ = 0.6 are 2031 K and 5.89 bar. With agent added to these lean flames, $C_6F_{12}O$, $C_3H_2F_3Br$, and C_2HF_5, have peak T_{ad} which are 331 K, 589 K, and 473 K higher than the uninhibited case, occurring at X_a = 0.025, 0.035, and 0.055 (for $C_3H_2F_3Br$, the peak value of T_{ad} is 20 K higher than that of the uninhibited stoichiometric methane–air flame, while for C_2HF_5 and $C_6F_{12}O$ it's about 100 K and 140 K lower). The increase in T_{ad} is due to the higher enthalpy of formation of the reactant mixture, and the stable product species (e.g., CO_2, HF, etc.); that is, with regard to the thermodynamics, the agents have fuel-like properties. In contrast, T_{ad} decreases by roughly 5 K for every 1% of added CF_3Br. For the pressure rise, the equilibrium results again show an increase in ΔP_{max} with addition of each agent, reaching a peak near the X_a for which [X]/[H] = 1 (at $X_a \approx$ 0.06, 0.02, 0.11, and 0.055 for CF_3Br, $C_6F_{12}O$, $C_3H_2F_3Br$, and C_2HF_5). For Φ = 0.6, however, both the relative and absolute pressure rise are much bigger than for Φ = 1, with equilibrium ΔP_{max} increasing by nearly 50% with addition of $C_6F_{12}O$, $C_3H_2F_3Br$, or C_2HF_5. In the experiments, the pressure rise was again always lower than the equilibrium value (i.e., $\lambda < 1$). For example, for X_a = 0, ΔP_{max} was 3.35 bar, or 43% lower than the equilibrium value, or λ = 0.57, which is much lower than the case of Φ = 1 and X_a = 0, for which λ = 0.91 (as discussed previously [64], slower flames are more strongly influenced by buoyancy-induced quenching). With addition of the agents, however, the behavior for Φ = 0.6 is different from that for Φ = 1. For the lean flames, λ often increases as X_a increases, as compared to the Φ = 1 case for which λ decreases. With regard to the peak experimental pressure rise, addition of $C_6F_{12}O$, $C_3H_2F_3Br$, or C_2HF_5 yielded a ΔP_{max} of 7.36 bar, 5.81 bar, or 6.96 bar, at X_a of 0.02, 0.03, or 0.06. These values are 2.2, 1.7, and 2.1 times the ΔP_{max} for the uninhibited system (3.35 bar). In contrast, addition of CF_3Br at X_a = 0.005 extinguished the flame just after ignition, yielding ΔP_{max} = 0.22 bar.

The results for the explosion pressure in the 1.85 L chamber (for Φ = 0.6) clearly illustrate the combustion enhancement of the type observed in the FAA-ACT [3], whereas results for Φ = 1 do not adequately duplicate the behavior. Hence, reduced-scale explosion vessels, used to evaluate lean fuel–air systems, are a valuable tool for understanding the FAA-ACT results; for example, the measurements of ΔP_{max} highlight the increased heat release occurring with addition of the halon replacements to the lean system. More than just the higher explosion pressure with added agent, however, the higher extent of reaction with added agent (in the Φ = 0.6 case) implies a higher burning velocity with agent addition to the lean flames. To more clearly investigate this possibility, the burning velocity is calculated from the pressure rise data (as described above) to more clearly delineate the effect of the agents on the overall reactivity of the system.

3.3. Laminar burning velocity

The laminar burning velocity was measured for the stoichiometric (Φ = 1) and lean (Φ = 0.6) methane–air flames. Initial conditions were T_0 = 296 ± 2 K, and P_0 = 0.868 bar, 1 bar, and 1.13 bar, (to provide more data for the curve fit). For each agent, tests were conducted up to values of X_a for which $S_L \approx$ 6 cm/s (since buoyant distortion has been found to be minimal for S_L > 6 cm/s). For each value of Φ and X_a, tests were conducted at the three values of P_0, providing the fitting parameters $S_{L,0}$, α, and β in Eq. (7) above. From these, the burning velocity was obtained at ambient and compressed conditions, as listed in Table 1. The burning velocity of the inhibited flames for each of the agents is presented in Fig. 6 (Φ = 1, left frame; Φ = 0.6, right frame) as the normalized burning velocity (for a given Φ and agent, S_L at X_a is divided by S_L with X_a = 0). Results for each agent are illustrated with different style symbols; closed and open symbols represent data at standard (298 K, 1 bar) and compressed (400 K, 3 bar) conditions.

As Fig. 6 shows, for stoichiometric flames, adding each agent reduces S_L at all values of X_a, with a decreasing marginal effectiveness at higher X_a, as has been discussed previously [68,69]. The present measurements (for T_0 = 298 K) can be compared to results in the literature. For CF_3Br addition, the reductions in S_L are very close to the stretch-corrected, spherically propagating flame

Table 1
Initial conditions, fit parameters, burning velocities, adiabatic temperatures, and explosion pressures for uninhibited methane–air flames.

	Φ	
Φ	0.6	1.0
α	2.23	1.68
β	−0.42	−0.33
$S_{L,0}$	8.3	35.8
S_L (400 K, 3 bar)	10.0	44.5
T_{ad}	2031	2599
$\Delta P_{max,equil}$	5.89	7.94
$\Delta P_{max,exp}$	3.35	7.19

results of Osorio et al. [26]; for example, at $X_a = 0.01$ the present result of 15.0 cm/s compares to Osorio et al.'s value of 14.9 cm/s. Linteris et al. [22,70] measured the burning velocity of flames inhibited with CF_3Br and C_2HF_5 using a Mache-Hebra burner (for values of S_L down to about 10 cm/s). In general, the present results are lower (including the uninhibited case), by roughly 4 cm/s, although the normalized values of S_L from the present data are in good agreement with those in Refs. [22,70], generally within ±5% at $X_a \leqslant 0.03$ and ±15% at higher concentrations.

On a molar basis, $C_6F_{12}O$ requires 1/2 as much as C_2HF_5 for a comparable reduction in S_L, and $C_3H_2F_3Br$, about 1/3 as much. The performance of $C_3H_2F_3Br$ and CF_3Br are roughly equivalent (on a molar basis), although CF_3Br is slightly more effective for $X_a < 0.01$, and $C_3H_2F_3Br$ for $X_a > 0.01$. This is consistent with cup burner results (heptane) [31,71] for which $C_3H_2F_3Br$ was found to have a lower minimum extinguishing concentration (2.6%) than CF_3Br (2.9%), and $C_6F_{12}O$ required roughly 50% more than CF_3Br (4.5%). Comparison of the results at ambient ($T_0 = 298$ K, $P_0 = 1$ bar) vs. compressed ($T_0 = 400$ K, $P_0 = 3$ bar) conditions shows that while the compressed flames have an uninhibited value of S_L about 14% higher, the reduction in normalized S_L with added agents is about 2% less for the compressed flames than for the ambient flames at low values of X_a, and 4% less at high values of X_a. This can be compared to flame inhibition by CO_2, for which the calculated normalized reduction in S_L at $T_0 = 353$ K as compared to $T_0 = 298$ K was 8%, 4%, and 0.3% lower at $X_a = 0.03$, 0.07, and 0.15 [70]. That is, for these initially stoichiometric flames, these changes in the unburned gas conditions do not appear to significantly affect the inhibition kinetics of these agents.

For the lean ($\Phi = 0.6$) flames, the effects of added agents on S_L are different than at $\Phi = 1$. For $T_0 = 298$ K, $C_6F_{12}O$ and C_2HF_5 increase S_L by 32% and 13% at $X_a = 0.01$ and 0.03. That is, with $C_6F_{12}O$ or C_2HF_5 added to lean flames of methane–air, the mixture becomes more reactive, with significantly increased burning velocity: S_L is increased for all values of X_a up to about 0.025 for $C_6F_{12}O$, and 0.065 for C_2HF_5. In contrast, with CF_3Br addition to the lean flame (at $X_a = 0.005$), the mixture was not flammable when subject to the highest available ignition energy. (The dashed line in the right frame of Fig. 6 is included to illustrate the inerting nature of CF_3Br at $X_a = 0.005$ and is not intended to provide S_L values between those measured at $X_a = 0$ and $X_a = 0.005$.) The results for $C_3H_2F_3Br$ are intermediate between those of CF_3Br and the other agents: for $X_a = 0.01$, S_L decreases by 30%, but as X_a increases, S_L increases so that at $X_a = 0.02$ and 0.03, S_L is only about 10% lower than the uninhibited flame speed. Note that with $C_3H_2F_3Br$ addition to the lean flame, the measured S_L is never higher than with no agent. Apparently, the gas-phase catalytic radical recombination cycles of brominated species have a larger inhibition effect in the present flames than the promotion effect of the agent due to the increased temperature [16]. (Nonetheless, the present oxidizer is dry. With added water vapor, typical of ambient air, the results may be different, as discussed previously [12,16].) With $C_6F_{12}O$ addition, S_L drops rapidly above $X_a = 0.02$, and with C_2HF_5 addition, it drops slowly above $X_a = 0.03$. At the compressed condition, the peak enhancement in S_L with addition of $C_6F_{12}O$ and C_2HF_5 is larger by 47% and 24%, while the decrease in S_L with $C_3H_2F_3Br$ addition is less. (Note that from α and β in Table 1, the effect of compression is primarily caused by higher temperature, not pressure, which has a small effect for the present range of variation in T_0 and P_0.)

The present results illustrate that when added to lean premixed dry methane–air flames at low concentrations, the agents $C_6F_{12}O$ and C_2HF_5 actually increase the burning velocity, and for $C_3H_2F_3Br$ addition, the burning velocity is reduced slightly (about 10% at $X_a = 0.02$ or 0.03). These results, together with the measured higher explosion pressures in the presence of these agents, are consistent with the higher overpressure in the FAA-ACT. Under lean conditions in the FAA-ACT, exothermic reaction of the agent creates higher overpressure than with no agent, and apparently the reaction rate is not sufficiently slowed (or is actually increased) with agent addition, so as to reduce the overpressure. In contrast, addition of CF_3Br both reduces the reaction rate for all stoichiometries,

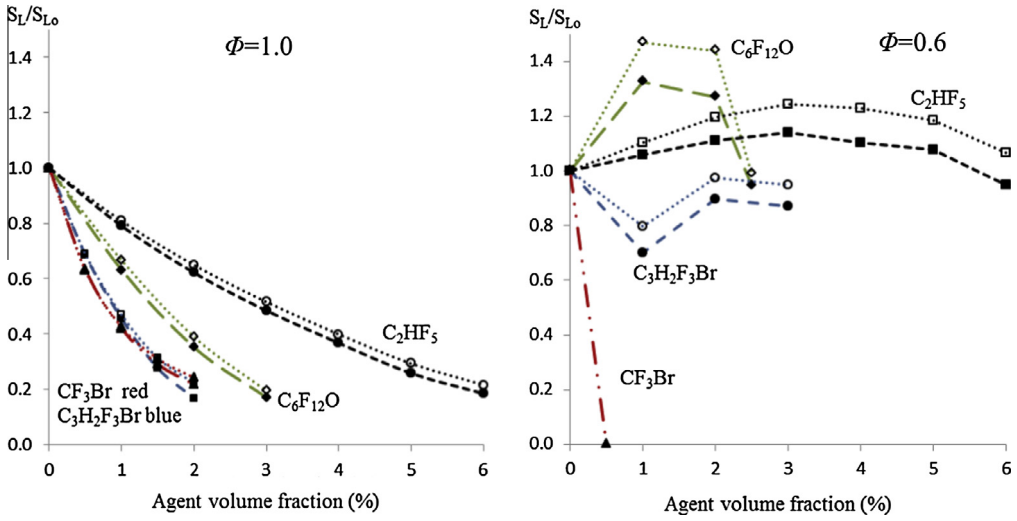

Fig. 6. Normalized burning velocity with agents added to methane–air flames ($\Phi = 1.0$, left frame; $\Phi = 0.6$, right frame). Dashed lines: $P_0 = 1$ bar, $T_0 = 298$ K; dotted lines: $P_0 = 3$ bar, $T_0 = 400$ K.

and causes no increase in the explosion pressure. These principles were predicted in numerical simulations, but the present results are experimental verification of the principles previously outlined [6,7,10,12], and the first to show increased flame speed of lean flames with added halon replacements.

4. Conclusions

Several potential halon replacements, for use in cargo-bay fire suppression, failed a mandated FAA performance test. To help understand their behavior, experiments were performed in a constant-volume combustion device (premixed methane–air system) to measure the peak pressure rise and burning velocity resulting from addition of the agents (CF_3Br, $C_6F_{12}O$, $C_3H_2F_3Br$, and C_2HF_5).

The influence of the agents on explosion pressure varied with agent type and concentration, as well as the initial stoichiometry of the methane–air mixture. For stoichiometric flames, addition of CF_3Br or $C_3H_2F_3Br$ reduced the peak pressure rise at all agent loadings; while $C_6F_{12}O$ and C_2HF_5 increased ΔP_{max} slightly at low loadings ($X_a \leqslant 0.02$ and 0.03), and reduced it at higher X_a. The equilibrium adiabatic temperatures initially increased (at low X_a) before dropping slightly with addition of CF_3Br or C_2HF_5 and significantly with addition of $C_3H_2F_3Br$ or $C_6F_{12}O$ to stoichiometric flames.

In lean ($\Phi = 0.6$) flames, however, addition of $C_6F_{12}O$, $C_3H_2F_3Br$, and C_2HF_5 all increased the pressure rise, with a peak pressure rise of about a factor of two above the uninhibited case, and occurring at agent loadings of 2–6%, depending upon the agent. In contrast, CF_3Br caused no increase in the ΔP_{max} at any condition. Pressure rises were always less than those predicted by equilibrium calculations, and the difference increased at higher agent loadings. The equilibrium adiabatic temperatures also increased with agent addition to lean flames (to values close to those of stoichiometric methane–air flames), and did not drop off as rapidly at higher X_a as did the experimentally determined ΔP_{max}.

All agents were found to reduce burning velocity of stoichiometric methane–air flames at the concentrations tested. CF_3Br and $C_3H_2F_3Br$ caused similar flame speed reductions (about 55% at $X_a = 0.01$), with CF_3Br slightly more effective at $X_a = 0.01$ and below, and $C_3H_2F_3Br$ more effective above. $C_6F_{12}O$ and C_2HF_5 were about 2/3 and 1/3 as effective as CF_3Br at reducing the burning velocity of stoichiometric flames.

For lean ($\Phi = 0.6$) methane–air flames at ambient initial temperature and pressure, addition of $C_6F_{12}O$ and C_2HF_5 at sub-inerting concentrations increased the burning velocity by 32% and 13%. That is, when added to lean flames, not only do they increase the explosion pressure, but they can also enhance the reactivity. Addition of $C_3H_2F_3Br$ slightly decreased the burning velocity (for $X_a \leqslant 0.03$), while addition of CF_3Br (at $X_a = 0.005$) inerted the mixture.

The data also provided burning velocities at compressed conditions ($P_0 = 3$ bar; $T_0 = 400$ K), for which agent addition to stoichiometric methane–air mixtures reduced the burning velocities slightly less than at ambient conditions ($P_0 = 1$ bar; $T_0 = 298$ K). For the lean ($\Phi = 0.6$) mixtures, addition of $C_6F_{12}O$ or C_2HF_5 increased the burning velocity (over uninhibited values) significantly (≈25–50%) more than for the ambient conditions. Similarly, the reduction in the burning velocity with $C_3H_2F_3Br$ addition was reduced at the compressed condition. (It should be noted that the present results are for dry mixtures. Addition of water vapor may affect the findings.) The experimental data indicate that the stronger enhancement at compressed conditions is due almost entirely to the higher temperature, not pressure.

In practice, when used to suppress fires, clean agents are typically added at concentrations high enough to extinguish the flames. In the present tests (and as apparently occurs in the FAA Aerosol Can test), however, when some halon replacements are added to lean mixtures (in closed vessels) at sub-inerting concentrations, they can enhance both the pressure rise and rate of reaction. These properties may be relevant for other situations as well, for example when halogenated hydrocarbons (as suppressants or inadvertently released agents) premix with air and a hydrocarbon fuel from some other source. Moreover, the present results show that reduced-scale combustion spheres are useful screening tools for the potential of halon replacements to cause unwanted combustion enhancement in full-scale use. In future work, detailed kinetic modeling will be used to interpret the role of the various chemical moieties on the inhibition or enhancement of lean premixed hydrocarbon flames.

Acknowledgments

We thank Dr. Kenji Takizawa at the National Institute of Advanced Industrial Science and Technology (AIST) for providing a list of parts used in his experimental setup. Conversations with him and with Dr. Valeri Babushok, Dr. Don Burgess, and Dr. Jeff Manion at NIST were very helpful. This research was supported by the Boeing Company and by an ARRA grant.

References

[1] The Montreal Protocol on Substances that Deplete the Ozone Layer as Adjusted and/or Amended in London 1990, Copenhagen 1992, Vienna 1995, Montreal 1997, Beijing 1999, UNEP.
[2] Revised Guidance Notes for Ozone Depleting Substances, Halon Phase-Out, EPA, 2008.
[3] J. Reinhardt, Behavior of Bromotrifluoropropene and Pentafluoroethane When Subjected to a Simulated Aerosol Can Explosion, FAA, 2004.
[4] J. Reinhardt, D. Blake, T. Marker, Development of a Minimum Performance Standard for Aircraft Cargo Compartment Gaseous Fire Suppression Systems, FAA, 2000.
[5] J. Reinhardt, International Aircraft Systems Fire Protection Working Group, FAA, 2006.
[6] G.T. Linteris, D.R. Burgess, F. Takahashi, V.R. Katta, H.K. Chelliah, O. Meier, Combust. Flame 159 (2012) 1016–1025.
[7] G. Linteris, F. Takahashi, V. Katta, H. Chelliah, O. Meier, IAFSS, 2011.
[8] V.I. Babushok, G.T. Linteris, O.C. Meier, Combust. Flame 159 (2012) 3569–3575.
[9] F. Takahashi, V.R. Katta, G.T. Linteris, O.C. Meier, Proc. Combust. Inst. 34 (2013) 2707–2717.
[10] G.T. Linteris, V.I. Babushok, P.B. Sunderland, F. Takahashi, V.R. Katta, O. Meier, Proc. Combust. Inst. 34 (2013) 2683–2690.
[11] F. Takahashi, V.R. Katta, G.T. Linteris, V. Babushok, P.T. Baker, Proc. Combust. Inst. (2014).
[12] G.T. Linteris, V.I. Babushok, D.R. Burgess, J.A. Manion, F. Takahashi, V. Katta, P.T. Baker, Unwanted combustion enhancement by $C_3H_2F_3Br$ (2-BTP) fire suppressant, Combust. Flame (2014) (in preparation).
[13] D. Burgess, M. Zachariah, P. Westmoreland, Prog. Energy Combust. Sci. 21 (1996) 453–529.
[14] V. Babushok, T. Noto, D.R.F. Burgess, A. Hamins, W. Tsang, Combust. Flame 107 (1996) 351–367.
[15] D.R. Burgess, A Chemical Kinetic Mechanism for 2-Bromotrifluoropropene (2-BTP) Flame Inhibition, 2014.
[16] V. Babushok, G.T. Linteris, D.R. Burgess Jr., P.T. Baker, Hydrocarbon flame inhibition by $C_3H_2F_3Br$ 2-BTP, Combust. Flame (2014) (accepted for publication).
[17] D. Burgess, M.R. Zachariah, W. Tsang, P.R. Westmoreland, Thermochemical and Chemical Kinetic Data for Fluorinated Hydrocarbons, NIST Technical Note 1412, 1995.
[18] V.I. Babushok, G.T. Linteris, O.C. Meier, J.L. Pagliaro, Combust. Sci. Technol. 186 (2014) 792–814.
[19] Y.N. Shebeko, V.V. Azatyan, I.A. Bolodian, V.Y. Navzenya, S.N. Kopylov, D.Y. Shebeko, E.D. Zamishevski, Combust. Flame 121 (2000) 542–547.
[20] S. Kondo, K. Takizawa, A. Takahashi, K. Tokuhashi, A. Sekiya, Fire Saf. J. 44 (2009) 192–197.
[21] G.T. Linteris, L. Truett, Combust. Flame 105 (1996) 15–27.
[22] G.T. Linteris, D.R. Burgess, V. Babushok, M. Zachariah, W. Tsang, P. Westmoreland, Combust. Flame 113 (1998) 164–180.
[23] Y. Saso, D.L. Zhu, H. Wang, C.K. Law, N. Saito, Combust. Flame 114 (1998) 457–468.
[24] J.C. Leylegian, D.L. Zhu, C.K. Law, H. Wang, Combust. Flame 114 (1998) 285–293.
[25] J.C. Leylegian, C.K. Law, H. Wang, in: Twenty-Seventh Symp. on Combust, 1998, pp. 529–536.

[26] C.H. Osorio, A.J. Vissotski, E.L. Petersen, M.S. Mannan, Combust. Flame 160 (2013) 1044–1059.
[27] C.H. Kim, O.C. Kwon, G.M. Faeth, J. Propul. Power 18 (2002) 1059–1067.
[28] X. Ni, W.K. Chow, Appl. Therm. Eng. 31 (2011) 3864–3870.
[29] J. Grigg, A. Chattaway, in: 12th Proceedings of Halon Options Technical Working Conference, 2002, pp. 1–10.
[30] Y. Zou, N. Vahdat, M. Collins, Ind. Eng. Chem. Res. 40 (2001) 4649–4653.
[31] B.P. Carnazza, J.G. Owens, P.E. Rivers, J.S. Schmeer, in: Papers from 1991–2006 Halon Options Technical Working Conferences, NIST SP 984-4.
[32] G. Lask, H.G. Wagner, Proc. Combust. Inst. 8 (1962) 432–438.
[33] V. Babushok, W. Tsang, Combust. Flame 123 (2000) 488–506.
[34] M. Metghalchi, J.C. Keck, Combust. Flame 38 (1980) 143–154.
[35] K. Takizawa, A. Takahashi, K. Tokuhashi, S. Kondo, A. Sekiya, Combust. Flame 141 (2005) 298–307.
[36] R. Stone, A. Clarke, P. Beckwith, Combust. Flame 114 (1998) 546–555.
[37] T. Iijima, T. Takeno, Combust. Flame 65 (1986) 35–43.
[38] J.E. Shephard, J.C. Krok, J.J. Lee, Spark Ignition Energy Measurements in Jet A, Explos. Dyn. Lab. Rep. FM 99e7, Calif. Inst. Tech., 1999.
[39] S.P. Marshall, S. Taylor, C.R. Stone, T.J. Davies, R.F. Cracknell, Combust. Flame 158 (2011) 1920–1932.
[40] M. Metghalchi, J.C. Keck, Combust. Flame 48 (1982) 191–210.
[41] P.G. Hill, J. Hung, Combust. Sci. Technol. 60 (1988) 7–30.
[42] B. Lewis, G. von Elbe, Combustion, Flames, and Explosions of Gases, 1961.
[43] K. Saeed, C.R. Stone, Combust. Flame 139 (2004) 152–166.
[44] K. Eisazadeh-Far, A. Moghaddas, J. Al-Mulki, H. Metghalchi, Proc. Combust. Inst. 33 (2011) 1021–1027.
[45] G.P. Smith, D.M. Golden, M. Frenklach, N.W. Moriarty, B. Eiteneer, C. Mikhail Goldenberg, T. Bowman, R.K. Hanson, S. Song, J. William, C. Gardiner, V.V. Lissianski, Z. Qin. <http://www.me.berkeley.edu/gri_mech/>.
[46] V.I. Babushok, D.R.F. Burgess, W. Tsang, A.W. Miziolek, Halon Replacements, 1995.
[47] S. Gordon, B.J. McBride, Computer Program for Calculation of Complex Chemical Equilibrium Compositions and Applications, N.R.P. 1311 (Ed.), NASA Glenn Research Center, Cleveland, OH, 1996.
[48] F.A. Williams, in: AGARD Conference Proceeding, 1975.
[49] M. Elia, M. Ulinski, M. Metghalchi, J. Eng. Gas Turb. Power 123 (2001) 190.
[50] A. Moghaddas, K. Eisazadeh-Far, H. Metghalchi, Combust. Flame 159 (2012) 1437–1443.
[51] D. Razus, V. Brinzea, M. Mitu, C. Movileanu, D. Oancea, Energy Fuels 26 (2012) 901–909.
[52] A.S. Huzayyin, H.A. Moneib, M.S. Shehatta, A.M.A. Attia, Fuel 87 (2008) 39–57.
[53] D.R. Dowdy, D.B. Smith, S.C. Taylor, Twenty-Third Symp. on Combust. (1990) 325–332.
[54] L.K. Tseng, M.A. Ismail, G. Faeth, Combust. Flame 95 (1993) 410–426.
[55] U.J. Pfahl, M.C. Ross, J.E. Shephard, Combust. Flame 123 (2000) 140–158.
[56] B.N. Taylor, C.E. Kuyatt, Guidelines for Evaluating and Expressing the Uncertainty of NIST Measurement Results, N.I.o.S.a. Technology (Ed.), 1994.
[57] M.I. Hassan, K.T. Aung, G.M. Faeth, Combust. Flame 112 (1998) 539–550.
[58] G. Rozenchan, D.L. Zhu, C.K. Law, S.D. Tse, Proc. Combust. Inst. 20 (2002) 1461–1469.
[59] O. Park, P.S. Veloo, N. Liu, F.N. Egolfopoulos, Proc. Combust. Inst. 33 (2011) 887–894.
[60] C.M. Vagelopoulos, F.N. Egolfopoulos, in: Twenty-Seventh Symp. on Combust., 1998.
[61] C.C.M. Luijten, E. Doosje, L.P.H. de Goey, Int. J. Therm. Sci. 48 (2009) 1213–1222.
[62] D. Razus, C. Movileanu, V. Brinzea, D. Oancea, J. Hazard. Mater. 135 (2006) 58–65.
[63] K.L. Cashdollar, I.A. Zlochower, G.M. Green, R.A. Thomas, M. Hertzberg, J. Loss Prevent. Process Ind. 13 (2000) 327–340.
[64] A.E. Dahoe, L.P.H. de Goey, J. Loss Prevent. Process Ind. 16 (2003) 457–478.
[65] G.F.P. Harris, Combust. Flame 11 (1967) 17–25.
[66] H.C. Hottel, A.F. Sarofim, Radiative Transfer, McGraw-Hill, 1967.
[67] S.S. Penner, J. Appl. Phys. 21 (1950) 685.
[68] G.T. Linteris, A.W. Miziolek, W. Tsang (Eds.), ACS Symposium Series 611, American Chemical Society, Washington, DC, 1995, pp. 260–274.
[69] T. Noto, V. Babushok, A. Hamins, W. Tsang, Combust. Flame 112 (1998) 147–160.
[70] G.T. Linteris, M.D. Rumminger, V.I. Babushok, W. Tsang, Proc. Combust. Inst. 28 (2000) 2965–2972.
[71] T.A. Moore, C.A. Weitz, R.E. Tapscott, in: Papers from 1991–2006 Halon Options Technical Working Conferences, NIST SP 984-4, 2001, pp. 551–564.